Bayesian Approach to Light-Curve Inversion of 2020 SO

Tanner S. Campbell

Department of Aerospace and Mechanical Engineering, Lunar and Planetary Laboratory, University of Arizona, Tucson, AZ, USA

Prof. Vishnu Reddy

Lunar and Planetary Laboratory, University of Arizona, Tucson, AZ, USA

Prof. Roberto Furfaro

Department of Systems and Industrial Engineering, Department of Aerospace and Mechanical Engineering, University of Arizona, Tucson, AZ, USA

Adam Battle

Lunar and Planetary Laboratory, University of Arizona, Tucson, AZ, USA

Peter Birtwhistle

Great Shefford Observatory, West Berkshire, UK

Tyler Linder

The Astronomical Research Institute, Ashmore, IL, USA

Scott Tucker

Starizona, Tucson, AZ, USA

Neil Pearson

Planetary Science Institute, Tucson, AZ, USA

ABSTRACT

Near-Earth Object (NEO) 2020 SO is thought to be a Centaur rocket booster from the Surveyor 2 mission to the Moon that was temporarily recaptured by the Earth. 2020 SO had close approaches to the Earth in December 2020 and February 2021, where it became bright enough (approximately 14 V magnitude) to be observed by Raven-class (~0.5 m) telescopes. In this paper, 2020 SO's spin state and reflective properties are estimated using ground-based photometric observations using five optical telescopes. The 95% Highest Posterior Density (HPD) region and Maximum A Posteriori (MAP) spin state and reflective properties of 2020 SO are estimated using Bayes' theorem via Markov Chain Monte Carlo (MCMC) sampling of a predictive light curve simulation. We estimate ten parameters at the start of an observation epoch: attitude quaternion (4), angular velocity vector (3), and diffusive/specular reflectivity parameters (3). The method of light curve inversion employed in this paper can be applied directly to other NEOs given photometric observations with a high enough temporal density and knowledge of some approximate physical properties of the object.

1. INTRODUCTION

Near Earth Object (NEO) 2020 SO was first discovered by the Pan-STARRS1 planetary defense survey in September 2020, two months before it was temporarily captured into Earth orbit. The recent expanse in focus of Space Domain Awareness (SDA) towards cislunar space (referred to as XDA) is only further justified by objects like 2020 SO. With a closest approach distance to the Earth (50,000 km) that edges perilously close to the

geosynchronous equatorial orbit (GEO) region and closer still to the GEO graveyard region, 2020 SO is a prime example of the type of object that warrants particular focus by the growing XDA community.

In this paper, we use data collected from five different telescope sites around the world to evaluate the performance of a Markov Chain Monte Carlo (MCMC) sampling-based inversion of 2020 SO's spin state and reflective properties. The light curve inversion is accomplished by specifying assumed distributions for each inverted parameter, then sampling from these distributions many times and using the predictive model to evaluate goodness of fit with the observed data.

Light curve inversion has been extensively studied as it applies to asteroids and other natural bodies ([10], [11], [16]), and the limitations regarding the observability of the inverted parameters and ill-posedness of the problem in general is well understood [5], [7]. These techniques are no less applied in the field of Space Situational Awareness (SSA) ([12], [13], [14], [15]), however the focus has almost exclusively been for characterization of shape or object type. There have been few (if any) attempts in the literature to apply these methods to a (partially) known object to assess the performance of a model-based approach with a comparison to real data.

2. HARDWARE AND METHODOLOGY

Table 1. Relevant parameters for the sensors used to collect data of 2020 SO.

Name	Location	Aperture (m)	FOV (arc-min)	Pixel Scale ($\frac{arcsec}{pixel}$)
RAPTORS II	Arizona, USA	0.61	21 x 16	0.56
Leo-20	Arizona, USA	0.52	81 x 81	2.4
CTIO	Cerro Tololo, Chile	1.0 0.61	9 x 9 24 x 24	1.04 1.4
IRTF	Hawaii, USA	3.2	1 x 1	0.12
GSO	Great Shefford, England	0.4	18 x 18	2.2

The photometric data used were collected with several optical sensor systems from multiple sites around the world. Some basic information for each of the sensors used can be found in Table 1. All observations were taken with an open/clear filter with the exception of the data from the NASA Infrared Telescope Facility (IRTF) which was captured with the MIT Optical Rapid Imaging System (MORIS) instrument using the Sloan Digital Sky Survey (SDSS) g' photometric filter with a band pass of 386 - 569 nm [6]. A summary of the observational circumstances is presented in Table 2.

Table 2. Summary of observation epoch and geometry for the collected data.

Name	Date (UTC)	Range (km)	V Mag (Pred.)	Phase Angle (°)	No. of Obs.
RAPTORS II	2021/01/31	351,500	16.4	25.9	1,004
Leo-20	2020/11/30	105,000	14.8	5.5	202
CTIO	2021/01/29	489,500	17.7	45.4	2,011
	2021/02/02	225,000	15.6	23.8	200
IRTF	2021/02/02	225,000	15.6	23.8	1,450
GSO	2020/11/30	105,000	14.8	5.5	315

In Bayesian statistics the estimated posterior likelihood of an event is predicated on the observational data available and any a priori assumptions about the system. For a parameter θ_i, any constraints or a priori beliefs are represented through a choice of prior distribution $p(\theta_i)$ as the likelihood of each choice of θ_i. Then, with the aid of a probabilistic model which associates all chosen parameters $\boldsymbol{\theta}$ to observations $\tilde{\boldsymbol{y}}$ via a likelihood function, Bayes' Rule allows estimation of the posterior conditional probability distributions $p(\boldsymbol{\theta}|\tilde{\boldsymbol{y}})$ [3].

$$p(\boldsymbol{\theta}|\tilde{\boldsymbol{y}}) = \frac{p(\tilde{\boldsymbol{y}}|\boldsymbol{\theta})p(\boldsymbol{\theta})}{\int p(\tilde{\boldsymbol{y}}|\boldsymbol{\theta})p(\boldsymbol{\theta})d\boldsymbol{\theta}} \quad (1)$$

The integral in the denominator equates to $p(\tilde{\boldsymbol{y}})$ and serves to normalize $p(\boldsymbol{\theta}|\tilde{\boldsymbol{y}})$ so that it may be considered a proper probability density function (PDF). Our aforementioned probabilistic model is represented in Eq. (1) by the term $p(\tilde{\boldsymbol{y}}|\boldsymbol{\theta})$, and is the likelihood of the realization of the observed data as a function of the parameter vector. In this research, the light curve simulation facilitates calculation of the observed data conditional likelihood. Direct computation of the posterior for an arbitrary choice of parameters is challenging in a low-dimensional well-posed problem and impossible in an ill-posed problem, so we employ a method known as Markov Chain Monte Carlo (MCMC) sampling. This allows for the generation of values from an estimated posterior distribution whereby more general statistics can be calculated to give an informative representation of the true posterior distribution.

3. RESULTS AND CONCLUSIONS

We ran a total of 35,000 iterations of the MCMC inversion, and used a partially uninformative prior via truncated uniform distributions. The shape of 2020 SO was defined as a homogeneous round-top cylinder shell with mass 2274.3 kg and dimensions 12.68 x 3.05 m [18]. Table 3 summarizes the relevant parameters associated with the distributions found through this test.

Table 3. Bayesian and frequentist statistics for the estimated posterior distributions of each parameter. Note: quaternion values are raw estimates and have not been re-normalized.

Variable	MAP	95% HPD	Mean	STD
q_1	0.015	[0.0071, 0.8257]	0.347	0.273
q_2	0.010	[-0.0007, 0.4859]	0.202	0.164
q_3	0.030	[0.0054, 0.4152]	0.180	0.138
q_4	0.985	[0.8016, 0.9996]	0.926	0.063
w_1	0.0011	[-0.0003, 0.0012]	0.0006	0.0005
w_2	0.0010	[-0.0002, 0.0011]	0.0005	0.0004
w_3	0.0009	[-0.0001, 0.0010]	0.0005	0.0004
ρ	0.998	[0.9140, 1.0000]	0.970	0.028
F_0	0.990	[0.5879, 0.9999]	0.833	0.140
d	0.575	[0.4150, 0.9181]	0.612	0.117

In Fig. 1 we took 1500 samples from the posterior distributions of each parameter, and computed the light curves. Then using the previously computed statistics, we can group the solutions into the 50% (dark gray) and 97.5% (light gray) HPD regions. We have also overlaid the measured light curve (dark gray) to show how it aligns with the predicted regions. As can be seen, except for a few of the faintest points which have the highest noise and uncertainty, the entire light curve falls within the 97.5% HPD region. This implies that we can be very confident that our model has done a good job of estimating the posterior distributions of 2020 SO's spins state and limited reflective properties.

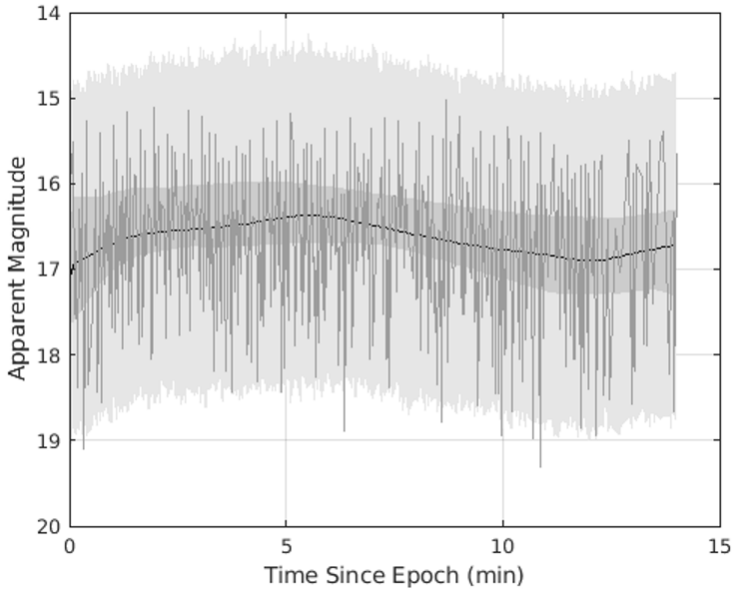

Fig. 1. The 50% (dark gray) and 97.5% (light gray) HPD regions in light curve phase space as estimated by 1500 random samplings from the posterior estimates generated with data taken from the RAPTORS II telescope on Jan. 31, 2021. The observed light curve of 2020 SO has been overlaid in dark gray.

In this paper, the 95% Highest Posterior Density (HPD) region and Maximum A Posteriori (MAP) spin state and reflective properties of 2020 SO are estimated using Bayes' theorem via Markov Chain Monte Carlo (MCMC) sampling. We show that it is possible to estimate posterior distributions of ten parameters at the start of an observation epoch: attitude quaternion (4), angular velocity vector (3), and diffusive/specular reflectivity parameters (3).

In the future we hope to improve this inversion process in a few ways. First, we plan to include the use of a surrogate Machine Learning (ML) model in place of the simulated light curve model. This will not only drastically reduce the computation time, but it will also allow for inversion of a higher fidelity physical model, that is to say one that can support inhomogeneous reflective properties. This improvement will allow us to further refine the parameter estimates, and probe into the existence of bimodal spin characteristics. Second, we will improve the long-term spin state propagation model to include primarily Earth tidal torques, as well as some other perturbing effects (solar radiation pressure, thermal emission pressure, etc) in order to cut down on the uncertainty growth during posterior propagation between observation epochs.

4. ACKNOWLEDGMENTS

This work is supported by NASA Near-Earth Object Observations program grant NNX17AJ19G (PI: Reddy).

Observations taken at CTIO were funded by the Astronomical Research Institute NASA grant 80NSSCC17K0124 (PI: Robert Holmes).

5. REFERENCES

[1] R. Andrae, M. Fouesneau, O. Creevey, C. Ordenovic, N. Mary, A. Burlacu, L. Chaoul, A. Jean-Antoine-Piccolo, G. Kordopatis, A. Korn, et al. Gaia Data Release 2 - First Stellar Parameters from Apsis. Astronomy & Astrophysics, 616:A8, 2018.

[2] M. Ashikmin and P. Shirley. An Anisotropic Phong Light Reflection Model. Univ. of Utah TR-UUCS-00-014, Salt Lake City, UT, 2000.

[3] R. Aster, B. Borchers, and C. Thurber. Parameter Estimation and Inverse Problems. Elsevier, 2018.

[4] C. Benson, D. Scheeres, and N. Moskovitz. Light Curves of Retired Geosynchronous Satellites. In 7th European Conference on Space Debris, volume 7, page 04, 2017.

[5] B. Calef, J. Africano, B. Birge, D. Hall, and P. Kervin. Photometric Sig- nature Inversion. In Unconventional Imaging II, volume 6307, page 63070E. International Society for Optics and Photonics, 2006.

[6] A. Gulbis, J. Elliot, F. Rojas, S. Bus, J. Rayner, W. Stahlberger, A. Tokunaga, E. Adams, and M. Person. A New Instrument for the IRTF: The MIT Optical Rapid Imaging System (MORIS). In AAS/Division for Planetary Sciences Meeting Abstracts# 42, pages 49–14, 2010.

[7] J. Hinks, R. Linares, and J. Crassidis. Attitude Observability from Light Curve Measurements. In AIAA Guidance, Navigation, and Control (GNC) Conference, page 5005, 2013.

[8] Jet Propulsion Laboratory. New Data Confirm 2020 SO to Be the Up- per Centaur Rocket Booster From the 1960's [Press Release]. 2020. URL https://www.jpl.nasa.gov/news.

[9] J. Junkins and H. Schaub. Analytical Mechanics of Space Systems. American Institute of Aeronautics and Astronautics, 2009.

[10] M. Kaasalainen and J. Torppa. Optimization Methods for Asteroid Lightcurve Inversion: I. Shape Determination. Icarus, 153(1):24–36, 2001.

[11] M. Kaasalainen, J. Torppa, and K. Muinonen. Optimization Methods for Asteroid Lightcurve Inversion: II. The Complete Inverse Problem. Icarus, 153 (1):37–51, 2001.

[12] R. Linares and J. Crassidis. Space-Object Shape Inversion via Adaptive Hamil- tonian Markov Chain Monte Carlo. Journal of Guidance, Control, and Dy- namics, 41(1):47–58, 2018.

[13] R. Linares, J. Crassidis, C. Wetterer, K. Hill, and M. Jah. Astrometric and Photometric Data Fusion for Mass and Surface Material Estimation using Re- fined Bidirectional Reflectance Distribution Functions-Solar Radiation Pres- sure Model. Technical report, PACIFIC DEFENSE SOLUTIONS LLC KIHEI HI, 2013.

[14] R. Linares, M. Jah, J. Crassidis, and C. Nebelecky. Space Object Shape Characterization and Tracking Using Light Curve and Angles Data. Journal of Guidance, Control, and Dynamics, 37(1):13–25, 2014.11. Gaia Collaboration et al. (2018b): Summary of the contents and survey properties.

[15] R. Linares, R. Furfaro, and V. Reddy. Space Objects Classification via Light- Curve Measurements Using Deep Convolutional Neural Networks. The Journal of the Astronautical Sciences, pages 1–29, 2020.

[16] K. Muinonen, J. Torppa, X. Wang, A. Cellino, and A. Penttila¨. Asteroid Lightcurve Inversion with Bayesian Inference. Astronomy & Astrophysics, 642:A138, 2020.

[17] Y. Takahashi, M. Busch, and D. Scheeres. Spin State and Moment of Inertia Characterization of 4179 Toutatis. The Astronomical Journal, 146(4):95, 2013.

[18] United Launch Alliance. Atlas V Launch Services Users Guide. Lockheed Martin Commercial Launch Services, 2010.

[19] B. Warner, A. Harris, and P. Pravec. The Asteroid Lightcurve Database. Icarus, 202(1):134–146, 2009.

[20] C. Wetterer, R. Linares, J. Crassidis, T. Kelecy, M. Ziebart, M. Jah, and P. Cefola. Refining Space Object Radiation Pressure Modeling with Bidirec- tional Reflectance Distribution Functions. Journal of Guidance, Control, and Dynamics, 37(1):185–196, 2014.